Benchmark Wall Heat Flux Data for a GO$_2$/GH$_2$ Single Element Combustor

William M. Marshall[*], Sibtosh Pal[†],
Roger D. Woodward[‡] and Robert J. Santoro[§]
Propulsion Engineering Research Center
and
Department of Mechanical and Nuclear Engineering
The Pennsylvania State University
University Park, Pennsylvania 16802

Wall heat flux measurements in a 1.5 in. diameter circular cross-section rocket chamber for a uni-element shear coaxial injector element operating on gaseous oxygen (GO$_2$)/gaseous hydrogen (GH$_2$) propellants are presented. The wall heat flux measurements were made using arrays of Gardon type heat flux gauges and coaxial thermocouple instrumentation. Wall heat flux measurements were made for two cases. For the first case, GO$_2$/GH$_2$ oxidizer-rich (O/F=165) and fuel-rich preburners (O/F=1.09) integrated with the main chamber were utilized to provide vitiated hot fuel and oxidizer to the study shear coaxial injector element. For the second case, the preburners were removed and ambient temperature gaseous oxygen/gaseous hydrogen propellants were supplied to the study injector. Experiments were conducted at four chamber pressures of 750, 600, 450 and 300 psia for each case. The overall mixture ratio for the preburner case was 6.6, whereas for the ambient propellant case, the mixture ratio was 6.0. Total propellant flow was nominally 0.27-0.29 lbm/s for the 750 psia case with flowrates scaled down linearly for lower chamber pressures. The axial heat flux profile results for both the preburner and ambient propellant cases show peak heat flux levels at axial locations between 2.0 and 3.0 in. from the injector face. The maximum heat flux level was about two times greater for the preburner case. This is attributed to the higher injector fuel-to-oxidizer momentum flux ratio that promotes mixing and higher initial propellant temperature for the preburner case which results in a shorter reaction zone. The axial heat flux profiles were also scaled with respect to the chamber pressure to the power 0.8. The results at the four chamber pressures for both cases collapsed to a single profile indicating that at least to first approximation, the basic fluid dynamic structures in the flow field are pressure independent as long as the chamber/injector/nozzle geometry and injection velocities remain the same.

[*] Graduate Student, Student Member AIAA.
[†] Senior Research Associate, Member AIAA.
[‡] Research Associate, Member AIAA.
[§] Professor of Mechanical Engineering, Member AIAA.

Nomenclature

q''	=	heat flux
C_p	=	specific heat
k	=	coefficient of thermal conductivity
$T_{surface}$	=	Temperature measured by surface thermocouple
$T_{recessed}$	=	Temperature measured by recessed thermocouple
Δx	=	distance between surface and recessed thermocouples
ρ	=	density
r_1	=	radial location of the surface thermocouple
r_2	=	radial location of the recessed thermocouple
h	=	heat transfer coefficient
P	=	Pressure

I.   Introduction

Experiments conducted to characterize wall heat flux for a gas/gas uni-element rocket chamber are presented and discussed. The work was conducted as part of a longer term NASA funded effort titled, "Focused Validation Data for Full Flow Staged Combustion Injectors." Full-flow staged-combustion (FFSC) cycle engines were recently considered for use as part of the NASA Reusable Launch Vehicle (RLV). In the FFSC cycle, oxidizer-rich gases drive the oxidizer turbopump and fuel-rich gases drive the fuel turbopump. Both propellants are then injected into the main combustion chamber as gases. The benefits that accompany the FFSC cycle are simplicity and increased thrust to weight ratio relative to other closed cycles. However, experience with gas/gas injectors is limited and, therefore, fundamental studies under uni-element conditions are necessary to understand the important physical/chemical mechanisms and to provide benchmark quality data for CFD code validation and verification.

Experiments conducted earlier in this effort focused on non-intrusive laser-based measurements for gas/gas injector flowfields.[1, 2] A significant portion of the hardware used for the experiments reported here was fabricated in the earlier stage of this program. Here, the goal was to characterize the chamber wall heat transfer for hot gas/gas injectors that use oxygen and hydrogen as the propellants. A heavily instrumented chamber for heat flux measurements was specifically designed and fabricated towards this end. Instrumentation included arrays of Gardon type heat flux gauges and coaxial thermocouples. Experiments were conducted for a shear coaxial injector element for both hot vitiated propellants as well as ambient temperature propellants.

In this paper, the experimental facility and setup are described first. The benchmark quality wall heat flux results obtained for all experiments are then presented, discussed and summarized.

II.   Experimental Facility and Setup

All rocket chamber combustion experiments were carried out at Penn State's Cryogenic Combustion Laboratory (CCL). This laboratory was established in 1989 to be the flagship facility for Penn State's Propulsion Engineering Research Center (PERC). In this section, the capabilities of the CCL are discussed first. This is followed by a description of the instrumented rocket chamber that was used for wall heat flux characterization experiments.

A. Cryogenic Combustion Laboratory (CCL)

The CCL is a unique university facility where researchers conduct work on representative rocket engine flow fields. The laboratory is designed based on a similar test cell at NASA Lewis Research Center (now the NASA Glenn Research Center at Lewis Field). The CCL, a remotely controlled laboratory, features a control room, diagnostic room and the test cell. The test cell, where the combustion experiment is housed, is isolated from the control and diagnostic rooms with reinforced concrete walls. For experimentation, the test cell's garage door is fully opened and the ventilation turned on to prevent the possible buildup of combustible materials. The diagnostic room located adjacent to the test cell is utilized for situating all the laser-based diagnostics. Optical ports between the diagnostics room and the test cell provide access into the test cell. The control room houses the computer control system that is used for timing the rocket firing. Video cameras with pan features enable remote visualizations of the test room. The operation of the entire system is designed with two levels of safety.

The CCL was initially operable for gaseous oxygen/hydrogen propellants. Liquid oxygen capability was initiated within a year of the laboratory's operation. Liquid hydrocarbon capability was brought on-line three years later. Finally airflow capability was brought on-line in early 1997. The propellant flowrate capabilities are tabulated Table 1.

Table 1. Flowrate capabilities of CCL.

| Propellant	Maximum Flowrate (lbm/s)
Gaseous Oxygen (GO$_2$)	1
Gaseous Hydrogen (GH$_2$)	0.25
Liquid Oxygen (LOX)	1
Liquid Hydrocarbon	0.5
Air	5 (can be upgraded to 16)

B. Overall Rocket Assembly

Wall heat flux characterization experiments for a shear coaxial injector element were conducted for both ambient temperature gaseous oxygen (GO$_2$)/gaseous hydrogen (GH$_2$) propellants as well as hot vitiated GO$_2$ and GH$_2$ propellants. For the latter series of experiments, the hot vitiated propellants were supplied using preburners. An instrumented rocket chamber with integrated preburners was designed and built for the studies. A cross section side view of the main rocket assembly, with preburner sections attached, is shown in Fig. 1. This configuration was used for the hot vitiated propellant experiments. For ambient temperature propellant experiments, the preburners were removed and room temperature gases were introduced through the cover plates as shown in Fig. 2. In terms of nomenclature, the hot vitiated propellant experiments will be referred to as the "preburner case", and the ambient temperature experiments as the "ambient propellant case".

The uni-element rocket design consists of a main rocket chamber and two gaseous GO$_2$/GH$_2$ propellant preburners, an oxidizer preburner which produces oxidizer-rich gases and a fuel preburner which produces fuel-rich gases. This configuration was chosen for study of main chamber injector elements of a full flow staged combustion cycle engine. The main rocket chamber is modular and can be easily configured to accommodate changes in chamber length or hardware configurations, such as sensor placement or injector design. The array of ports seen on both the preburners and main chamber are for pressure tap access. The chamber sections are held together with a hydraulic jack that allows for easy assembly and arrangement of the various sections. The preburners are designed to be bolted onto the main rocket chamber perpendicular with respect to the main axis of the main rocket chamber. Therefore, flow from the preburners turns 90° before being injected into the main rocket chamber through the study injector.

The main rocket chamber is a heat sink design made of oxygen-free high conductivity (OFHC) copper. The internal diameter (ID) of the main chamber is 1.5 in. Chamber length can be varied by inserting or removing blank chamber sections. For the experimental results reported here, the rocket chamber length was 11.25 in. The design allows for operational pressures of up to 1000 psia, and a water cooled nozzle allows for H$_2$/O$_2$ operation at near stoichiometric conditions (~5940°F (~6400 R)). The design of the water cooled nozzle allows for different
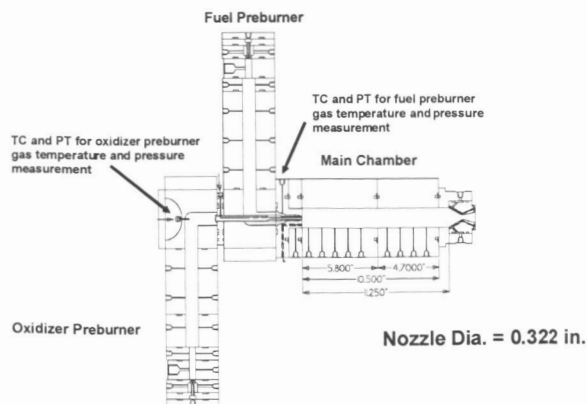
Fig. 1. Main chamber integrated with oxidizer-rich and fuel-rich preburners. TC: thermocouple; PT: Pressure Transducer.
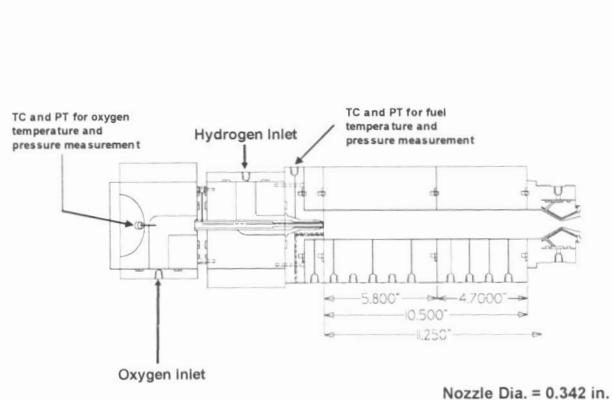
Fig. 2. Setup for ambient propellant experiments. TC: thermocouple; PT: Pressure Transducer.

American Institute of Aeronautics and Astronautics

diameter nozzles to be interchanged, thus providing the capability for changing the main chamber pressure for a given total propellant mass flowrate. The main chamber flow is ignited using a GH_2/GO_2 torch igniter.

The integrated preburners consist of an oxidizer preburner and a fuel preburner. The oxidizer preburner is operated oxidizer-rich and is fabricated from Monel, which was chosen for safety since Monel resists burning in an oxygen-rich environment. The fuel preburner is operated fuel-rich and is fabricated from oxygen-free high conductivity (OFHC) copper. Both preburners are designed based on a near-stoichiometric core/downstream dilution philosophy. The preburners consist of an impinging element injector located at the upstream end to provide near stoichiometric mixture ratios. This hot gas from the "stoichiometric core" is then diluted, with GH_2 for the fuel preburner and GO_2 for the oxidizer preburner. Flow from the preburners is then turned 90° before being injected through the study injector in the main rocket chamber, as can be seen in the Fig. 1. Both preburners have a 0.5 in. internal diameter (ID) upstream of the dilution injectors, and have an inner diameter of 1.0 in. from the dilution injectors to the main rocket injector. Each preburner chamber is 12 in. long, which corresponds to the length prior to the turn into the main rocket injector. Flows in the preburners are ignited using GH_2/GO_2 torch igniters.

For both preburners, the near-stoichiometric core injector is an impinging injector, whereas dilution is introduced through holes in the wall for radially inward injection. For the fuel preburner, the near-stoichiometric core impinging injector is a fuel centered pentad with four 30° centrally angled holes surrounding the central hole for fuel. In contrast, for the oxidizer preburner, the near-stoichiometric core impinging injector has six 20° angled holes surrounding the central hole for fuel. Both preburners operate with GH_2 flowing through the central element and GO_2 flowing through the angled holes.

In order to withstand the high temperatures of near stoichiometric flow conditions at the nozzle throat, a high flowrate water cooled nozzle was designed. The nozzle shape is a conical nozzle of 15° half angle, and is fabricated from OFHC copper. Water flow passages (15) along the nozzle wall are used for cooling the nozzle, especially the throat area. Water enters the nozzle via the water passages along the nozzle's radial edge, passes through the cooling passages, and is ejected from the nozzle through four stainless steel tubes silver soldered around the exit of the nozzle.

The water-cooled nozzle assembly is also modular in design, similar to the rocket chamber sections. Nozzles of different throat diameters can be interchanged, allowing for different chamber pressures for the same propellant flowrate. The nozzle is held by bolts that have been drilled out to weaken them so as to serve as a pressure relief for the chamber in case of rapid unexpected over-pressurization. The bolts are designed and have been tested to relieve chamber pressure when pressure rises above 1500 psia.

As discussed earlier, the propellants in the two preburners and the main chamber are ignited using three identical GO_2/GH_2 torch igniters (not shown in Fig. 1). In these igniters, GO_2 and GH_2 are injected off-axis into the igniter and are ignited using a spark plug driven by an oil furnace ignition transformer. Ignition is detected by a pressure rise in the igniter combustion chamber. The pressure rise in the igniter is checked before propellants are introduced to the main chamber and preburners. The hot gases from the igniters flow into the integrated rocket assembly and ignite the propellant flows in the preburners and main chamber.

C. Shear Coaxial Injector

The modular design of the rocket assembly allows for different injector geometries to be studied. For this investigation, a shear coaxial injector design was considered. This injector was designed to be integrated with the
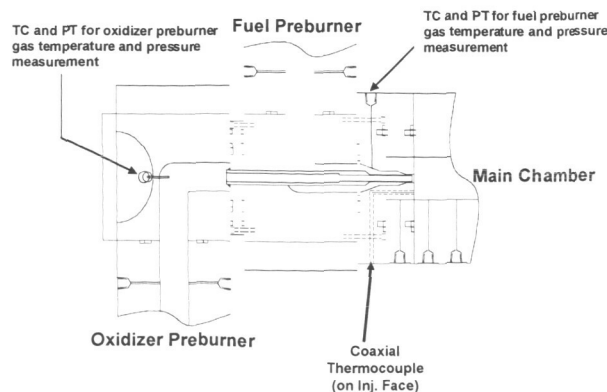

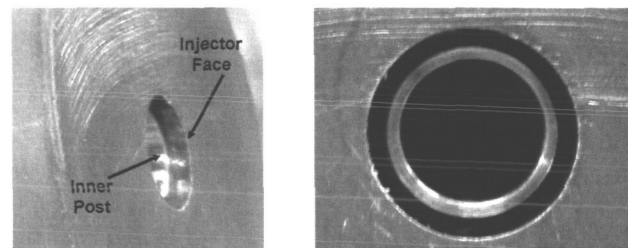**Fig. 3.** Closeup of shear coaxial injector element. TC: thermocouple; PT: Pressure Transducer.

Fig. 4. Photographs of injector. The oxidizer post was concentric to within 0.001 in.

American Institute of Aeronautics and Astronautics

preburners and main rocket chamber. The injector was a scaled down design of full scale FFSC engine flow conditions, with oxygen-rich gas supplied through the central post inner passage, and fuel-rich gas supplied through the annular passage. The post of the injector was made from Monel because of its compatibility with oxygen. Based on the design conditions, the central post inner diameter was 0.207 in., and the annular passage inner and outer diameters were 0.247 in. and 0.295 in., respectively. The integration of the injector with the main chamber/preburners assembly is evident through inspection of Figs. 1 and 2, with further details of the injector provided in Fig. 3.

Extreme care was exercised in the manufacturing and assembling of the injector. The injector dimensions reported earlier are accurate to less than 0.001 in. For all assembling procedures, the concentricity of the oxidizer post was rigorously established to be less than 0.001 in. Photographs of the injector are depicted in Fig. 4 to provide the reader with a visualization of the injector.

For the experiments, the goal was to have the post tip slightly recessed with respect to the injector face for both the preburner and ambient propellant cases. The post tip was initially recessed 0.060 in. from the injector face. For the preburner case experiments, the co-flowing hot gases from the preburners thermally expand the post length. Estimation and measurements (not discussed here) indicate that post growth due to thermal expansion is 0.043 in. which places the post tip with respect to the injector face during hot-fire to be 0.017 in. In contrast, for the ambient propellant case, the post does not expand due to thermal expansion since the propellants are at ambient temperature.

The propellant temperature at main chamber injection is another key parameter that is critical in terms of boundary condition specification for the experiments. Although the preburners are designed for complete combustion of the propellants, there is severe heat loss to the preburner combustor walls. Consequently, CEA[3] calculated temperatures are not accurate for prescribing the boundary conditions at the main study injector. For all experiments, Type K thermocouples were inserted into the flow at two positions. A thermocouple was inserted into the oxidizer preburner flow through the port shown in Fig. 3 located at the back turn area of the oxidizer preburner. Another thermocouple was inserted in the annular region of the fuel flow 1.5 in. upstream of the injector face. This port is also seen in Fig. 3 on the top part of the figure.

To further ascertain the temperature of the oxidizer flow, a separate thermocouple instrumented oxidizer post was fabricated. For this injector post, a thermocouple was snaked in to measure the temperature of the oxidizer flow nominally 0.5 in. upstream from the injector face in the oxidizer post. A small number of tests were first conducted with this instrumented injector. Subsequent experiments that concentrated on wall heat flux measurements did not have this thermocouple since the presence of the thermocouple affects the flow. In summary, the injector temperatures are well characterized.

D. Flow Conditions

The target flow conditions for the experiments are summarized in Tables 2 and 3 for the preburner and ambient propellant cases, respectively. For both cases, experiments were carried out at four chamber pressure conditions,

Table 2. Nominal run conditions for preburner case.*

	Mass Flowrate (lbm/s)				Uncertainty
	P_c=300 psia	P_c=450 psia	P_c=600 psia	P_c=750 psia	(%)
GH_2 (Fuel Preburner)	0.0139	0.0209	0.0278	0.0348	2.71
GO_2 (Fuel Preburner)	0.0152	0.0228	0.0304	0.0380	1.05
GH_2 (Ox. Preburner)	0.00048	0.00072	0.00096	0.0012	1.45
GO_2 (Ox. Preburner)	0.0797	0.1196	0.1594	0.1993	2.71
Fuel Preburner O/F	1.09	1.09	1.09	1.09	2.89
Ox. Preburner O/F	165	165	165	165	3.06
Overall O/F	6.6	6.6	6.6	6.6	4.18
Main Injector Nominal Conditions					
Ox. Velocity (ft/s)	466	466	466	466	
Fuel Velocity (ft/s)	2609	2609	2609	2609	
Velocity Ratio (V_f/V_o)	5.6	5.6	5.6	5.6	
Mom. Flux Rat. (F/O)	3.41	3.41	3.41	3.41	
Mom. Ratio (F/O)	2.03	2.03	2.03	2.03	

* Table provides nominal target conditions.

Table 3. Nominal run conditions for ambient propellant case.*

	Mass Flowrate (lbm/s)				Uncertainty (%)
	P_c=300 psia	P_c=450 psia	P_c=600 psia	P_c=750 psia	
GH$_2$	0.0164	0.0246	0.0328	0.041	2.5
GO$_2$	0.0984	0.1476	0.1968	0.246	2.5
Overall O/F	6.0	6.0	6.0	6.0	3.54
	Main Injector Nominal Conditions				
Ox. Velocity (ft/s)	254	254	254	254	
Fuel Velocity (ft/s)	1126	1126	1126	1126	
Velocity Ratio (V_f/V_o)	4.43	4.43	4.43	4.43	
Mom. Flux Rat. (F/O)	1.24	1.24	1.24	1.24	
Mom. Ratio (F/O)	0.74	0.74	0.74	0.74	

* Table provides nominal target conditions.

viz. 300, 450, 600 and 750 psia. Note that in these two tables, nominal target flow conditions are presented. Actual flow conditions differ slightly from these target values.

For the preburner case (Table 2), the fuel and oxidizer preburners were targeted to operate at mixture ratios of 1.09 and 165, respectively, with an overall mixture ratio (i.e. total GH$_2$ to total GO$_2$ flowrate ratio) of 6.6. The fuel and oxidizer temperatures at the main study injector are nominally 1000°F and 800°F, respectively (based on thermocouple measurements described earlier). A nozzle with a throat diameter of 0.322 in. (Fig. 1) was used for all the preburner case experiments. Experiments were conducted at the four target chamber pressures by scaling the propellant mass flowrates linearly as is evident in Table 2. Nominal injection velocities and pertinent non-dimensional ratios are also included in the table. Uncertainties in the individual and overall mass flowrates are also presented.

For the ambient propellant case (Table 3), the target mixture ratio was 6.0. A nozzle with a throat diameter of 0.342 in. (Fig. 2) was used for all the ambient propellant case experiments. Experiments were conducted at the four aforementioned target chamber pressures by again scaling the propellant mass flowrates. Note that in comparison to the preburner case, the overall mixture ratios are similar, but the non-dimensional ratios, i.e. velocity ratio, momentum ratio and momentum flux ratio (F/O) are all higher for the preburner case. Based on these differences and the higher propellant temperatures for the preburner case, the combustion zone length in the main chamber would be shorter for the preburner case which would clearly contrast axial wall heat flux characteristics between the two cases.

E. Flow System Configuration and Timing

At the CCL, both the GO$_2$ and GH$_2$ systems are split into primary and secondary circuits. For the preburner case, the primary circuit was used to supply the primary flow to the respective preburner (i.e. hydrogen to fuel preburner or oxygen to oxidizer preburner). The secondary circuit was used to feed the secondary flows to the respective preburners (i.e. oxygen to fuel preburner or hydrogen to oxidizer preburner). For the simpler ambient propellant case, only the primary propellant circuits were employed. Propellants to the igniters were supplied independently from gas bottles located in the test cell. Flowrates are controlled by critical orifices. For the experiments reported here, a typical test was three seconds in duration.

F. Heat Flux Transducer and Coaxial Thermocouple Instrumentation

The main chamber was instrumented with arrays of Gardon type heat flux gauges and coaxial thermocouples supplied (and mounted) by MEDTHERM Corporation. For the heat flux gauge,
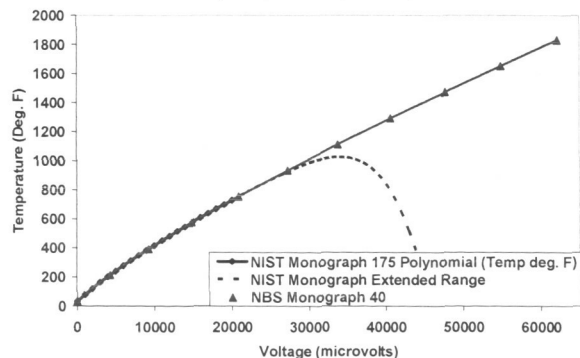
Fig. 5. Type-T thermocouple response. Both NIST monograph 175 and NBS monograph 40 responses are included in figure.

6

the sensing area is flat with a nominal diameter of 0.125 in. The heat flux gauges have a maximum measurement range of 17.4 BTU/in^2·s. The flat tip of these gauges was not contoured to the curvature of the chamber. In contrast, the tip of a coaxial thermocouple has a diameter of 0.1 in. with a smaller sensing area. The coaxial thermocouple has two Type-T thermocouples located at the tip and at a recessed location nominally 0.25 in. from the tip. The coaxial thermocouples were press fit into the main chamber wall and the tip was contoured to match the curvature of the chamber. In terms of actual measurements, the heat flux gauge provides a voltage measurement that is directly proportional to heat flux. The coaxial thermocouple provides temperature measurements at the two locations, i.e. tip and recessed locations.

Fig. 6. Heat flux and coaxial thermocouple locations in main chamber.

The wall heat flux can then be evaluated using the appropriate heat flux equation (planar or cylindrical coordinates).

The coaxial thermocouples use Type-T junctions. The temperature versus voltage response for Type-T thermocouples is shown in Fig. 5. In the figure, both NIST monograph 175[4, 5] and NBS monograph 40[6] responses are shown. The maximum suggested temperature for use of NIST monograph 175 is 750°F. The extended polynomial for higher voltages also included in the figure shows that at higher temperatures, the polynomial is inapplicable. NBS monograph 40 shows a near-linear response for higher temperatures but is less accurate in the lower temperature range (<750°F). In the current work, temperatures were evaluated from the raw voltage measurements using NIST monograph 175 for temperatures up to 750°F, and NBS monograph 40 was used at higher temperatures.

The instrumented main chamber has two sections that are 5.8 and 4.7 in. long as shown in Fig. 6. For the experiments reported here, the longer section was located upstream of the shorter section. Axial locations for instrumentation are indicated in the figure. In the longer section, both heat flux gauges and coaxial thermocouples are located at 0.5 in. axial intervals, whereas in the shorter section, the first three instrumentation pairs are spaced at 0.5 in. intervals and the rest at 1 in. intervals. In the longer section, multiple instrumentation (2 each) is present at the 1.0, 3.0 and 5.0 in. axial locations. For axial locations with one coaxial thermocouple and one heat flux gauge, the instrumentation is clocked at 180°, whereas for axial locations with two coaxial thermocouples and two heat flux gauges, the instrumentation is separated at 90°.

Photographs of the rocket assembly are shown in Fig. 7 to illustrate the instrumentation on the main chamber. In the photograph on the left, the instrumentation seen in the bottom area of the main chamber is the linear array of heat flux gauges. The array of coaxial thermocouples can be seen on the top part of the rocket. The extra three coaxial thermocouples at the 1.0, 3.0 and 5.0 in. axial locations are also seen in both photographs. However, the extra three heat flux gauges at the same three axial locations but diametrically opposed to the extra three coaxial
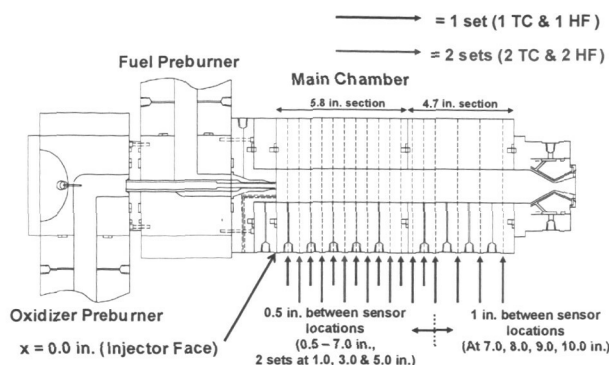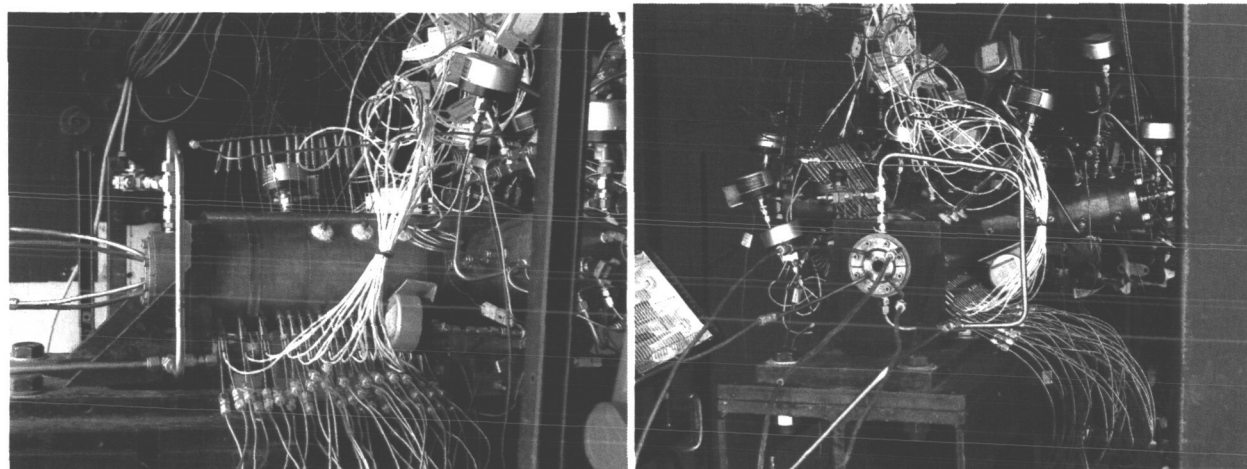

Fig. 7. Photographs of the experimental setup.

thercouples are not seen in either photograph. Note that for the heat flux gauges, cooling water is required, and the inlet and outlet copper tubes are also seen in the photographs.

The injector face is also instrumented with a single coaxial thermocouple that is located 0.5 in. from the centerline. The location of this thermocouple can be seen in the schematic of Fig. 3.

Each coaxial thermocouple provides a transient temperature measurement at the hot wall and at a point 0.25 in. back from the wall. Since both these temperatures increase with time in a heat-sink rocket chamber, the transient heat equation needs to be solved to evaluate the wall heat flux. A three-node (r_1, r_2 and a centered node) discretized approximate procedure was employed to evaluate the wall heat flux using the appropriate OFHC copper values for the thermal conductivity, k, specific heat, C_p, and density, ρ. For the coaxial thermocouple located on the injector face, planar equations were solved, whereas for the wall mounted coaxial thermocouples, cylindrical equations were solved. Note that the results obtained using this approximate procedure are relatively close to those obtained using higher number of nodes, and is nominally 6% higher than that obtained using a quasi steady state assumption.

The uncertainty analysis for the instrumentation indicates that for the heat flux gauges, the uncertainty in the heat flux measurement is 0.52 BTU/in^2·s. Similarly, the heat flux estimated from the two temperature measurements of a coaxial thermocouple has an uncertainty of 0.11 BTU/in^2·s for the wall locations and an uncertainty of 0.107 BTU/in^2·s for the injector face location.

III. RESULTS AND DISCUSSION

The wall heat flux results for the preburner case and ambient propellant case experiments are presented and discussed in this section. For both sets of experiments, multiple rocket firings (up to three) were carried out at four target chamber pressures, viz. 300, 450, 600 and 750 psia. In addition to the target conditions listed in Tables 2 and 3, heat flux measurements were also made for off-target conditions for the preburner case. For these tests, the stoichiometry of both the oxidizer and fuel-preburners were varied to ascertain the sensitivity of the wall heat flux measurements to nominally 5% changes in preburner operation. Measurements of wall heat flux were made using both heat flux gauges and coaxial thermocouples. As will be evident from reading the discussion in this section, the heat flux gauges in some cases exhibited "strange behaviors" and in general the signals were "noisy". In contrast, the heat flux estimated from the coaxial thermocouple paired temperature measurements of wall and recessed locations showed high fidelity. Consequently, the majority of the results presented here are from the coaxial thermocouple instrumentation.

A. Instrumentation Behavior

The time traces of select coaxial thermocouples and heat flux gauges for a representative 600 psia chamber pressure preburner case test are shown in Figs. 8 and 9, respectively. In Fig. 8, five sets of coaxial thermocouple temperature measurements are shown. For each coaxial thermocouple, the thicker line corresponds to the surface temperature measurement whereas the thinner line is the recessed temperature measurement. In terms of nomenclature in the figure, for example, the first trace labeled TC-3.0-0-F denotes that the thermocouple is at the 3.0 in. axial location, at 0° degrees (angle is defined with respect to major array of coaxial thermocouples) and the measurement is for the front (surface) thermocouple. All temperature traces are well behaved and are not noisy. During the steady state portion of the firing, the temperatures rise steadily due to the heat sink nature of the chamber design. The two coaxial thermocouples located at the 3.0 in. axial location are nearly identical suggesting that the chamber flow is concentric. The heat flux was evaluated from the coaxial thermocouple temperature measurements using the procedure (with steady state assumptions) described earlier and by averaging between 5.8 and 6.2 s (corresponding to the end portion of each firing). It should be noted that all instrumentation was not functional for all rocket firings. The surface thermocouple junction for coaxial thermocouples breaks occasionally and the contact has to be remade. The procedure is relatively simple but for nearly all the firings, a few instruments are non-functional. Heat flux versus time traces for five heat flux gauges for the same firing are presented in Fig. 9. The nomenclature here is again similar. HF denotes heat flux gauge, the next number is the axial location of the gauge and the third number denotes the angle location. In contrast to the coaxial thermocouple measurements, the heat flux gauge measurements are relatively noisy.[**] Also some heat flux gauges exhibit strange behaviors.

[**] In discussions with MEDTHERM Corp. following the test series, they stated the observed behavior had not previously been experienced for these heat flux gauges in terms of the observed noise. They suggested that ground loop or electric signal pickup between the heat flux sensors may have been the source of the problem as all the heat gauges had a common ground contact through the main chamber wall. These potential sources for the observed noise have not been investigated further.
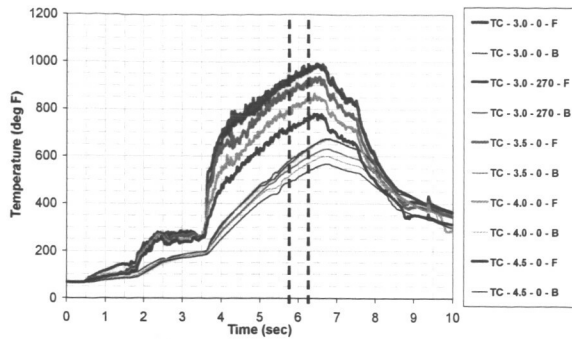
Fig. 8. Coaxial thermocouple temperature traces (representative) for a 600 psia test (preburner case). Nomenclature TC-X-Y-Z; X = axial position in inches, Y = angle in degrees with respect to major array of coaxial thermocouples (TC), Z = surface measurement location (F) or recessed measurement location (B).
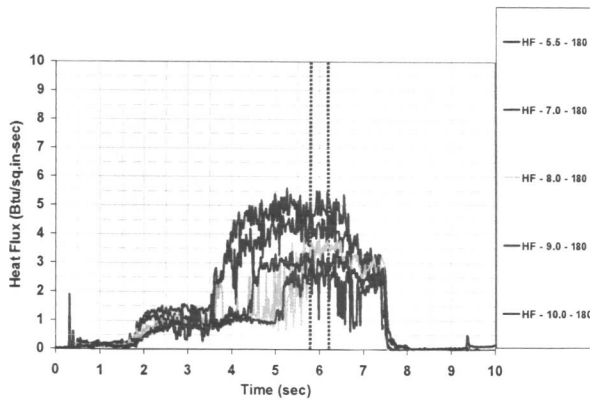

Fig. 9. Heat flux traces (representative heat flux gauges) for a 600 psia test (preburner case).
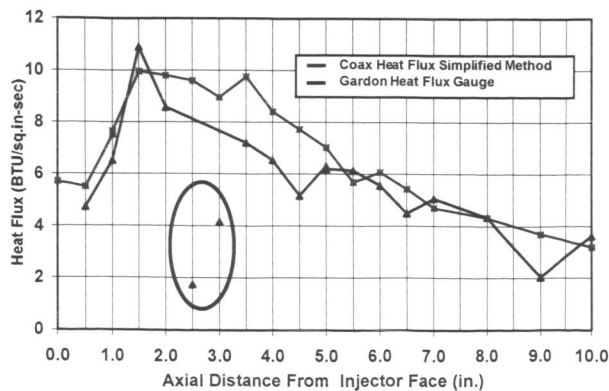

Fig. 10. Representative (750 psia case) heat flux versus axial distance (preburner case). Measurements from heat flux gauges and coaxial thermocouples are included (results averaged between 5.8 and 6.2 s of firings). Note that results from two heat flux gauges are questionable.
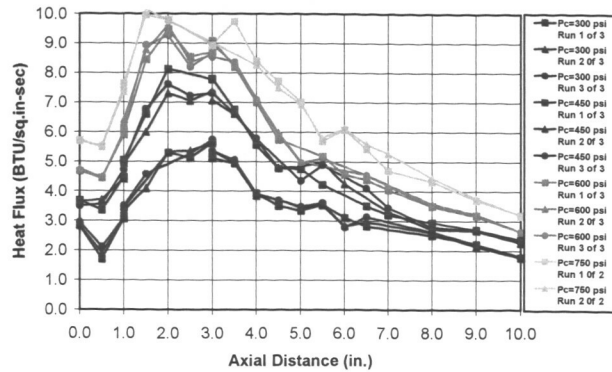
Fig. 11. Heat flux versus axial distance for four chamber pressure cases (preburner case). Results of multiple (2-3) tests at each pressure case are included in the figure. Note that the uncertainty in the coaxial thermocouple gauges is calculated to be 0.107 Btu/in^2·s.
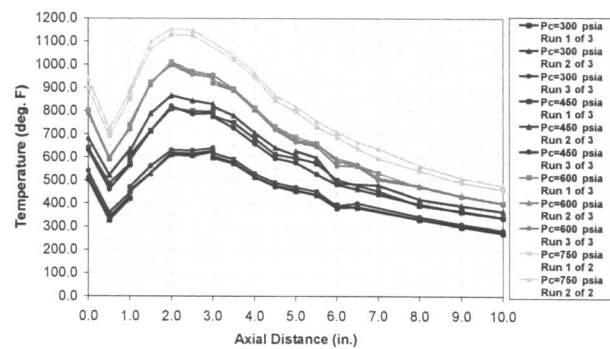
Fig. 12. Wall temperature versus axial distance for four chamber pressure cases (preburner case). Results of multiple (2-3) tests at each pressure case are included in the figure.
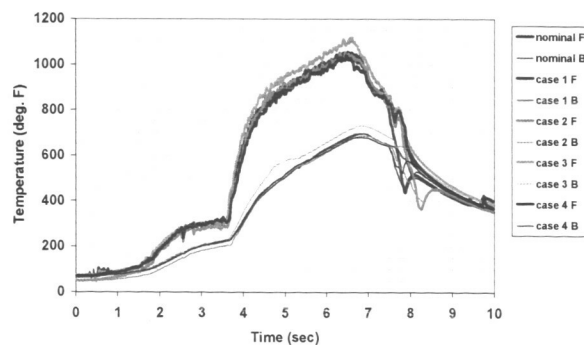
Fig. 13. Representative (2.0 in. axial location) coaxial thermocouple temperature measurements for off-target condition tests (preburner case). Nominal chamber pressure of 600 psia.

For example, the heat flux time trace at the 5.5 in. axial location is relatively noisy but still realistic. In contrast, the gauge at the 8.0 in. axial location is extremely noisy and does not show an increase in heat flux at the same time that the 5.5 in. gauge does. In summary, the heat flux gauges were more problematic and prone to failure than the coaxial thermocouple instrumentation.

The axial profile of wall heat flux from the two types of instruments is plotted in Fig. 10 for a representative 600 psia preburner case firing. The results show that except for two heat flux gauges that were erratic, there is qualitative agreement between the two results. Note that in the plot, the heat flux measurement (coaxial thermocouple) at the 0.0 in. axial location is from the coaxial thermocouple on the injector face. The heat flux increases with axial distance from the injector face until about the 3.0 in. location, and then monotonically decreases with further distance. Due to the erratic and noisy nature of the heat flux gauge measurements, all results presented hereafter focus on the coaxial thermocouple measurements.

B. Preburner Case Results

The full set of preburner case wall heat flux axial profiles are presented in Fig. 11. Multiple firing results (2-3) at the four target pressure conditions of 750, 600, 450 and 300 psia are included in the figure. Qualitatively, all profiles are similar, and agreement between multiple runs at the same chamber pressure is good. The heat flux increases with axial distance, is at its highest value between nominally 2.0 and 3.0 in., and then decreases with further axial distance. The peak heat flux value is about 10.0 BTU/in^2·s for the 750 psia pressure, and about 5.5 BTU/in^2·s for the 300 psia pressure. In the figure, the absence of a data point indicates that for that particular firing, the coaxial thermocouple instrument was not functioning. The results also show that when two instruments at the same axial location (1.0, 3.0 and 5.0 in.) were functioning, the results are relatively close indicating that for the preburner case, the flow is concentric.

The similarity in shape of the heat flux profiles at the four chamber pressures is to be expected since the injection velocities, and therefore all the non-dimensional ratios (see Table 2) are the same for all pressures. Further discussion on this point is presented in a later sub-section on pressure scaling.

The corresponding wall temperatures for all preburner case firings are presented in Fig. 12. The wall temperature profile is also similar to the wall heat flux profiles. The maximum temperature is again between the 2.0 and 3.0 in. locations.

C. Preburner Case Results for Off-Target Conditions

Experiments were also carried out at off-target flow conditions (~600 psia) to determine the sensitivity of the resulting wall heat flux on 5% type changes in preburner flowrates. The actual flow conditions for these off-target cases are presented in Table 4. The baseline target mixture ratios for the fuel and oxidizer preburners were 1.09 and 165, respectively. The four off-target condition cases were operated with the mixture ratios in the preburners varied between high (H) and low (L) numbers with respect to the baseline condition. For example, the fuel and oxidizer preburners were operated at mixture ratios of 1.22 (H) and 173 (H), respectively for the case 3 off-target condition. The actual flowrates to the preburners presented in the table for the four off-target cases helps in understanding how the preburner mixture ratios were varied with respect to the baseline condition.

The results of this sensitivity study are presented in Fig. 13 where the temperature traces of the coaxial thermocouple at the 2.0 in. axial location are plotted. Note that this axial location is characterized by the highest

Table 4. Summary of off-target preburner case flow conditions for 600 psia case.

	Mass Flowrate (lbm/s)					
	Target	**Nominal**	Case 1	Case 2	Case 3	Case 4
GH$_2$ (FP)	0.0278	**0.0277**	0.0298	0.0266	0.0268	0.0295
GO$_2$ (FP)	0.0304	**0.0305**	0.03017	0.03262	0.03266	0.02978
GH$_2$ (OP)	0.00096	**0.00094**	0.000950	0.001067	0.000965	0.001073
GO$_2$ (OP)	0.1594	**0.1567**	0.1667	0.1502	0.1667	0.1529
FP O/F	**1.09**	**1.10**	**1.01 (L)**	**1.23 (H)**	**1.22 (H)**	**1.01 (L)**
OP O/F	**165**	**168**	**176 (H)**	**141 (L)**	**173 (H)**	**143 (L)**

FP: Fuel preburner; OP: Oxidizer preburner
L: Low; H: High

Table 5. Summary of off-target preburner case results for 2.0 in. axial location.

	Mass Flowrate (lbm/s)					
	Target	Nominal	Case 1	Case 2	Case 3	Case 4
FP O/F	1.09	1.10	1.01 (L)	1.23 (H)	1.22 (H)	1.01 (L)
OP O/F	165	168	176 (H)	141 (L)	173 (H)	143 (L)
Heat Flux (BTU/in²·s)		**8.5**	**8.55**	**8.72**	**8.91**	**8.29**

FP: Fuel preburner; OP: Oxidizer preburner
L: Low; H: High

level of measured heat flux. The temperature traces show that except for the case 3 off-target case, the remaining three temperature traces are near-identical. For case 3, the temperature is higher by nominally 40°F. The corresponding averaged heat flux numbers for the off-target cases are summarized in Table 5. Clearly, the results indicate that the wall heat flux is not extremely sensitive to changes in preburner operating conditions. Alternately, since the uncertainty in mass flowrates to the preburners (see Table 2) is not as severe as the flowrate changes made for the off-target cases, it is stated that the uncertainty of the heat flux measurements for the target cases is relatively small.

To provide a quantitative estimate of the uncertainty in the measured heat flux in terms of "goodness" of the reported data is not straightforward as there is no analytical expression to relate the uncertainty in flow rates, pressures and temperatures to the heat flux observed for any single run. Given this difficulty, the approach taken here is to use the off-target cases as if they represented random events that result from the uncertainty in the measured mass flow rates. Note that variation used in the off-target flow conditions (±5%) exceeds the maximum uncertainty in the O/F (≈±3%). Thus, the present analysis is a conservative estimate of the uncertainty in the heat flux data.

The approach is to estimate the 95% confidence interval using the student t distribution for the heat flux results of the off-target flow condition runs.[7] In this approach the probability distribution is assumed to be Gaussian with a mean value, μ, and a standard deviation, σ. Of course, the mean value or the standard deviation are not known in advance as determining them requires running a large number of tests. Instead the mean value, X_{avg}, is estimated as the average of the four heat flux measurements listed in Table 5 for the four off target flow conditions and then the standard deviation S_x based on this mean value is estimated. The mean value is given as:

$$X_{avg} = (1/N)\Sigma X_i \tag{1}$$

where N is the number of samples ($N = 4$ for this case) and X_i are the heat flux measurements tabulated in Table 5. The standard deviation can be estimated as:

$$S_x = \{\Sigma(1/(N-1))(X_i - X_{avg})^2\}^{1/2} \tag{2}$$

Using these estimations for the mean value and the standard deviation, the 95% confidence limits for a single test result can be estimated as:

$$S_{x, 95} = t\, S_x \tag{3}$$

where t is the student t distribution coefficient for N-1 degrees of freedom (in this case $t = 3.182$). For an individual heat flux measurement, this results in a value for $S_{x, 95} = 0.55$ Btu/in²·s (6.3%). The 95% confidence limits for the sample set of four runs, $S_{xavg,95}$ can be estimated as:

$$S_{xavg, 95} = t\, S_x/\sqrt{N} \tag{4}$$

which equals 0.27 Btu/in²·s (3.1%) for the data in Table 5. Again, it should be noted that these estimates are very conservative as the off-target flow conditions exceed the 95% confidence limits for the flow measurements. Nonetheless, they do provide some concrete estimates to guide comparison between measurement and prediction.
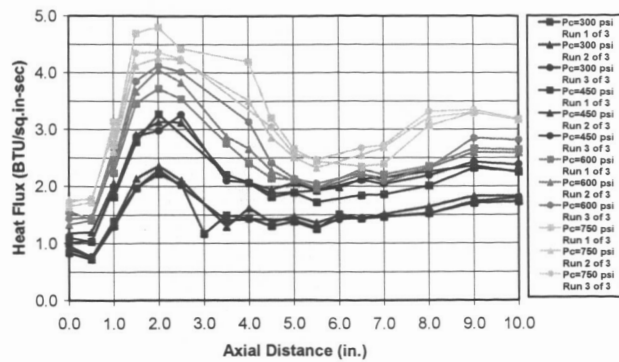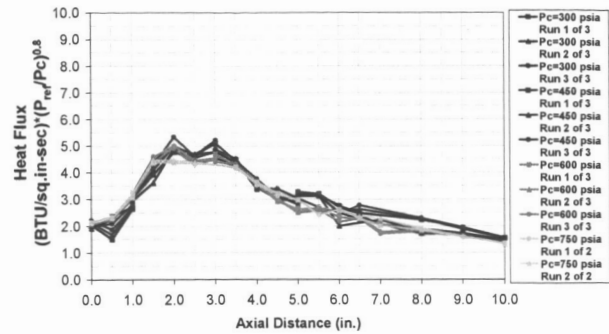
Fig. 14. Heat flux versus axial distance for four chamber pressure cases (ambient propellant case). Results of multiple (2-3) tests at each pressure case are included in the figure. Note that the uncertainty in the coaxial thermocouple gauges is calculated to be 0.107 Btu/in^2·s.

Fig. 16. Heat flux (scaled with respect to (300 psia/P$_c$)$^{0.8}$) versus axial distance for four chamber pressure cases (preburner case). Results of multiple (2-3) tests at each pressure case are included in the figure.

Fig. 15. Wall temperature versus axial distance for four chamber pressure cases (ambient propellant case). Results of multiple (2-3) tests at each pressure case are included in the figure.
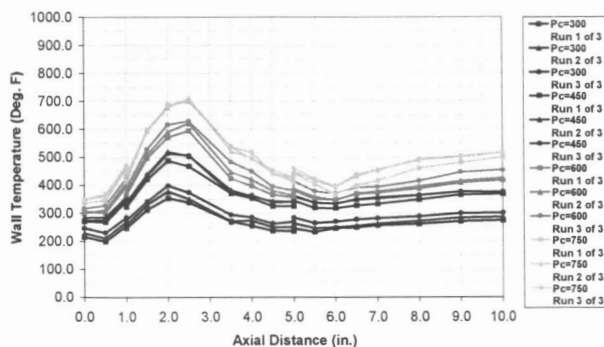
Fig. 17. Heat flux (scaled with respect to (300 psia/P$_c$)$^{0.8}$) versus axial distance for four chamber pressure cases (ambient propellant case). Results of multiple (2-3) tests at each pressure case are included in the figure.
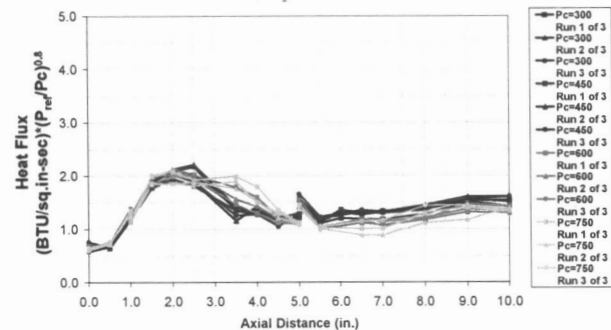
D. Ambient Propellant Case Results

The measured wall heat flux profiles for the ambient propellant case experiments are depicted in Fig. 14. Multiple firing results (2-3) at the four target pressure conditions of 750, 600, 450 and 300 psia are included in the figure. Qualitatively, all profiles are similar, and agreement between multiple runs at the same chamber pressure is good. The heat flux increases with axial distance, is at its highest value between nominally 2.0 and 3.0 in., and then nominally decreases with further axial distance. The peak heat flux value is about 4.7 BTU/in^2·s for the 750 psia pressure, and about 2.2 BTU/in^2·s for the 300 psia pressure. In the figure, the absence of a data point indicates that for that particular firing, the coaxial thermocouple instrument was not functioning. The results also show that when two instruments at the same axial location (1.0, 3.0 and 5.0 in.) were functioning, the results are close to within 0.5 BTU/in^2·s (at 5.0 in. axial location) which is not as good as that observed for the preburner case. This may be due to the fact that the shear coaxial injector pressure drop for ambient propellant operation is relatively low and therefore flow history effects (side entry of propellants with respect to main flow direction) may be present. However, the results again show similarity in shape of the heat flux profiles at the four chamber pressures since the injection velocities, and therefore all the non-dimensional ratios (see Table 3) are the same for all pressures.

The corresponding wall temperatures for all ambient propellant case firings are presented in Fig. 15. The wall temperature profile is also similar to the wall heat flux profiles. The maximum temperature is again between the 2.0 and 3.0 in. locations.

The peak wall heat flux levels measured for the ambient propellant case are roughly a factor of two lower than those measured for the preburner case. Total propellant flowrates and overall mixture ratios are respectively within

12
American Institute of Aeronautics and Astronautics

5% and 10% of each other for the preburner and ambient propellant cases. This is highlighted by the observation that at the furthest downstream measurement location (10.0 in.) where the flow is nearly one-dimensional, the wall heat flux values are nearly the same for both cases (see Figs. 14 and 11). Clearly, the higher injector momentum flux value which promotes mixing, and the higher initial propellant temperatures for the preburner case yields a shorter combustion zone with characteristically higher wall heat flux in the near injector region.

E. Pressure Scaling of Results

Inspection of empirical heat transfer correlations available in the literature such as the Bartz[9] or Dittus-Boelter[9] indicate that the heat transfer coefficient, h, is proportional to pressure to the power 0.8. For the results discussed here, the temperature of the combustion products (~6000°F) is significantly larger than the measured axial wall temperature variation of ~600°F (preburner case at 750 psia). Therefore, to first approximation, the wall heat flux should also scale with $P^{0.8}$ since the wall heat flux is proportional to the product of heat transfer coefficient, h, and the temperature differential between the fluid and the wall.

The measured wall heat flux profiles for the preburner (Fig. 11) and ambient propellant (Fig. 14) cases are plotted with the aforementioned pressure scaling term in Figs. 16 and 17, respectively. Here, all pressures are referenced to the 300 psia pressure. The collapse of the results to a single profile is remarkable and indicates that at least to first approximation, the basic fluid dynamic structures in the flowfield are pressure independent as long as the chamber/injector/nozzle geometry and injection velocities remain the same.

IV.   CONCLUSIONS

Benchmark quality wall heat flux data sets for CFD code validation and verification were obtained for a gas/gas shear coaxial injector element. The experiments were conducted carefully to provide well documented boundary conditions. The experiments were complemented with a rigorous analysis to define uncertainty limits for all propellant mass flowrates and heat flux measurements. The experimental program benefited from weekly discussions with NASA MSFC colleagues with CFD expertise. Clearly, in terms of lessons learned, obtaining benchmark quality data sets for CFD code validation requires close interactions between experimentalists and CFD researchers.

Acknowledgments

References

[1]Marshall, W. M., Cramer, J. M., Pal, S., and Santoro, R. J., "Experimental Characterization of Gas/Gas Injector Flowfields," 38th JANNAF Combustion Subcommittee Meeting, Destin, FL, April 8-12, 2002.

[2]Marshall, W. M., Cramer, J. M., Pal, S., and Santoro, R. J., "Experimental Characterization of Gas-Gas Injector Flowfields," Propulsion Engineering Research Center, Penn State, Fourteenth Annual Symposium, State College, PA, December 10-11, 2002.

[3]McBride, B. J. and Gordon, S., Computer Program for Calculation of Complex Equilibrium Compositions and Applications, NASA Reference Publication 1311, 1996.

[4]Omega Engineering, Inc., Temperature Handbook, Vol. MM, "Revised Thermocouple Reference Tables, Type T Reference Tables N.I.S.T. Monograph 175 Revised to ITS-90," p. Z-223, 1999.

[5]Omega Engineering, Inc., Temperature Handbook, Vol. MM, "ITS-90 Thermocouple Direct and Inverse Polynomials," p. Z-199, 1999.

[6]Caldwell, F. R., "Thermocouple Materials," NBS Monograph 40, March 1962.

[7]Coleman H. W. and Steele, W. G., Experimentation and Uncertainty Analysis for Engineers, 2nd edition John Wiley and Sons, New York, 1999.

[8]Bartz, D. R., "Turbulent Boundary-Layer Heat Transfer from Rapidly Accelerating Flow of Rocket Combustion Gases and of Hot Air," Advances in Heat Transfer, Vol. 2, 1965.

[9]Özişik, M. N., Heat Transfer: A Basic Approach, McGraw Hill Inc., New York, 1985.

American Institute of Aeronautics and Astronautics